JGR Atmospheres

RESEARCH ARTICLE
10.1029/2021JD034960

Non-Marine Sources Contribute to Aerosol Methanesulfonate Over Coastal Seas

Shengqian Zhou[1], Ying Chen[1,2], Adina Paytan[3], Haowen Li[1], Fanghui Wang[1], Yucheng Zhu[1], Tianjiao Yang[1], Yan Zhang[1,2], and Ruifeng Zhang[4]

[1]Shanghai Key Laboratory of Atmospheric Particle Pollution Prevention, Department of Environmental Science & Engineering, Fudan University, Shanghai, China, [2]Institute of Eco-Chongming (IEC), Shanghai, China, [3]Institute of Marine Sciences, University of California Santa Cruz, Santa Cruz, CA, USA, [4]School of Oceanography, Shanghai Jiao Tong University, Shanghai, China

Key Points:

- The concentrations of aerosol methanesulfonate over coastal East China Sea and the Gulf of Aqaba exhibit distinct seasonal variations
- Terrestrial sources make a substantial contribution to methanesulfonate in autumn and winter over coastal East China Sea
- Air transport height greatly affects the linkage between aerosol methanesulfonate and phytoplankton biomass

Supporting Information:

Supporting Information may be found in the online version of this article.

Correspondence to:

Y. Chen,
yingchen@fudan.edu.cn

Citation:

Zhou, S., Chen, Y., Paytan, A., Li, H., Wang, F., Zhu, Y., et al. (2021). Non-marine sources contribute to aerosol methanesulfonate over coastal seas. *Journal of Geophysical Research: Atmospheres*, *126*, e2021JD034960. https://doi.org/10.1029/2021JD034960

Received 23 MAR 2021
Accepted 30 SEP 2021

Author Contributions:

Conceptualization: Shengqian Zhou, Ying Chen
Data curation: Ying Chen, Adina Paytan
Formal analysis: Shengqian Zhou
Funding acquisition: Ying Chen
Investigation: Shengqian Zhou, Ying Chen, Haowen Li, Fanghui Wang, Yucheng Zhu, Tianjiao Yang
Methodology: Shengqian Zhou, Ying Chen
Project Administration: Ying Chen, Yan Zhang
Resources: Shengqian Zhou, Ying Chen, Adina Paytan
Software: Shengqian Zhou
Supervision: Ying Chen, Yan Zhang
Validation: Shengqian Zhou, Ying Chen
Visualization: Shengqian Zhou

Abstract Methanesulfonate (MSA) in the marine boundary layer is commonly considered to be solely contributed by the oxidation of ocean-derived dimethyl sulfide (DMS) and often used as an indicator of marine biogenic sources. But whether this judgment is valid in coastal seas and how the validity is affected by air mass transport history have been less discussed. Based on multi-year observations of aerosol MSA in the coastal East China Sea (ECS) and the Gulf of Aqaba (GA), as well as the analysis of air mass transport pattern and exposure to ocean surface phytoplankton biomass, we found that terrestrial sources made a non-negligible contribution to MSA over the ECS but not over the GA. The abundant MSA in winter over the coastal ECS was likely associated with substantial emissions of volatile organic sulfur compounds from both anthropogenic and natural sources in eastern China and significant terrestrial transport influenced by the East Asian Monsoon. Good correlations between aerosol MSA and air mass exposure to surface phytoplankton biomass were established by removing the influence of terrestrial transport and confining the air transport height within boundary layer, which makes it possible to construct parameterizations for obtaining the spatiotemporal distributions of marine biogenic aerosol components using satellite ocean color datasets.

1. Introduction

Marine biogenic sources contribute substantially to atmospheric gaseous and particulate components and exert significantly environmental and climatic effects (Carpenter et al., 2012; O'Dowd et al., 2004). Ocean organism-derived dimethyl sulfide (DMS) is the largest natural source of sulfur-containing gases emitted to the atmosphere (Watts, 2000), which can be oxidized and transformed into sulfate aerosols and thereby impact the cloud condensation nuclei (CCN) and downward radiation over the ocean (Barnes et al., 2006; Charlson et al., 1987). A part of DMS will be oxidized to form methanesulfonic acid/methanesulfonate (MSA) by both gaseous and aqueous phase reactions in the atmosphere (Barnes et al., 2006; Hoffmann et al., 2016). MSA is one of the most abundant secondary organic aerosol (SOA) components in marine environment, and its ratio to non-sea-salt SO_4^{2-} (nss-SO_4^{2-}) ranges from less than 10^{-2} to near 1 (Bates et al., 1992; Facchini et al., 2008; Gondwe et al., 2004). Thermodynamic calculation and global modeling have shown that MSA in the atmosphere also plays a potential role in the formation and growth of aerosols (Bork et al., 2014; Hodshire et al., 2019; Zhao et al., 2017).

The more vital role of MSA in atmospheric chemistry research is being used as a tracer for marine biogenic sources (Savoie et al., 2002), because it is generally considered to be solely from the biogenic DMS over the ocean. For example, the concentration of biogenic SO_4^{2-} is usually estimated by multiplying MSA concentration by the nss-SO_4^{2-}/MSA ratio measured in the pristine marine atmosphere (Gao et al., 1996; Park et al., 2017; Savoie & Prospero, 1989; Zhang et al., 2014) or calculated by a temperature-dependent function (Bates et al., 1992; Mihalopoulos et al., 2007; Nakamura et al., 2005; Yang et al., 2009). However, the quantitative relationship between MSA and biogenic SO_4^{2-} depends on the oxidation pathway of DMS, which is influenced by many factors in addition to temperature, such as DMS oxidants, relative humidity, vanadium in aerosols, and cloud cover (Barnes et al., 2006; Gaston et al., 2010; Hoffmann et al., 2016; Huang et al., 2015; Sorooshian et al., 2015). Moreover, recent studies have pointed out that aerosol MSA may not be chemically stable under the exposure of high concentration of OH radical due to heterogenous oxidation

Writing – original draft: Shengqian Zhou
Writing – review & editing: Shengqian Zhou, Ying Chen, Adina Paytan, Ruifeng Zhang

(Kwong et al., 2018; Mungall et al., 2017). Therefore, considerable caution should be taken when using MSA as a quantitative tracer.

In contrast to a large amount of studies exploring the chemical pathways of MSA, its sources have drawn little attention yet. The uniqueness of marine biogenic source for aerosol MSA over the ocean is still generally accepted (Mungall et al., 2017). However, it should be noted that the precursors of MSA (DMS, dimethyl disulfide (DMDS), dimethyl sulfoxide, etc.) can also be derived from terrestrial sources including tree emission (Vettikkat et al., 2020), biomass burning (Meinardi, 2003), salt marsh emission (Dacey et al., 1987; Wang & Wang, 2017) and anthropogenic sources such as pulp and paper industry, manure, and rayon/cellulosics manufacture (Giri et al., 2015; Lee & Brimblecombe, 2016; Zang et al., 2017). For example, it has been estimated that the vegetation and soil contribute 3,470 and 868 Gg S a^{-1} of DMS and DMDS, and the estimated global fluxes from pulp and paper industries were 1,462 and 273 Gg S a^{-1} for DMS and DMDS, respectively (Lee & Brimblecombe, 2016). The contribution of terrestrial sources to total emissions of DMS and DMDS is approximate 21% on a global scale (Lee & Brimblecombe, 2016). High concentrations of MSA have been observed in inland areas of China, which were primarily from anthropogenic sources or soil emission (Li et al., 2021; Yuan et al., 2004). Additionally, the size distribution of MSA mainly in fine particles suggests that it may be transported over a long distance (Jung et al., 2014; Kerminen et al., 1997; Sorooshian et al., 2015). Therefore, terrestrial sources may have a non-negligible contribution to the aerosol MSA over coastal seas, but this issue has not been thoroughly studied.

Coastal seas are significantly affected by atmospheric transport from adjacent continent. Meanwhile, they often appear strong biological activities and subsequently high emissions of DMS and other biogenic components (Spracklen et al., 2008; Yang et al., 2015), which may greatly affect aerosol formation and properties. It is necessary to differentiate between land- and ocean-derived MSA and unravel the influence of marine biogenic sources on aerosol components in these regions. A good correlation between MSA and sea surface phytoplankton biomass can be the evidence for predominant influence of marine biogenic source on MSA, since ocean-derived DMS is a degradation product of dimethylsulphoniopropionate (DMSP) predominantly synthesized by phytoplankton (Bullock et al., 2017; Sunda et al., 2002).

In this paper, aerosol MSA concentrations and seasonal variations were characterized based on multi-year observations at two coastal sites, Huaniao Island of the East China Sea and the Gulf of Aqaba in Red Sea. Combined with the satellite remote-sensing chlorophyll *a* (Chl-*a*) concentrations, meteorological data, and air mass backward trajectories, we revealed the factors influencing MSA concentrations and identified the dominant sources of MSA at different sites and seasons. Based on these results, we established good correlations between MSA and surface phytoplankton biomass by removing the influence of terrestrial input and confining air transport height within boundary layer, which would be very useful for exploring the linkage between lower atmosphere and surface ocean, obtaining the spatiotemporal distribution of marine biogenic aerosols and exploring their climate effects.

2. Materials and Methods

2.1. Sampling and Chemical Analysis

Huaniao Island (HNI, 30.86°N, 122.67°E) is located in the coastal East China Sea (ECS) east to the Yangtze River Estuary (YRE) with humid climate. The ECS is a eutrophic sea and has high phytoplankton biomass, while YRE is one of the most densely populated regions in the world with enormous anthropogenic emissions to the atmosphere (Figure 1). By contrast, the Gulf of Aqaba (the GA, 29.52°N, 34.92°E) is an oligotrophic sea surrounded by the deserts of Arabia, Sinai, Sahara and Negev with low rainfall (~30 mm per year) and relatively low population density (Chen et al., 2007) (Figure 1). Total suspended particles (TSP) were collected at HNI from 2013 to 2018 and in the GA from 2003 to 2005 using high-volume particle samplers with sampling durations of several hours to 3 days. The samples were stored at −20°C prior to further analysis. Detailed information about totals of 385 and 96 samples collected respectively at HNI and the GA is listed in Table 1. Water soluble ions (MSA, SO_4^{2-}, Na^+, etc.) were extracted using deionized water and analyzed by ion chromatography (DIONEX ICS-3000 for HNI samples and DIONEX DX-500 for the GA samples) generally within 6 months after the sampling. The detailed sampling procedure

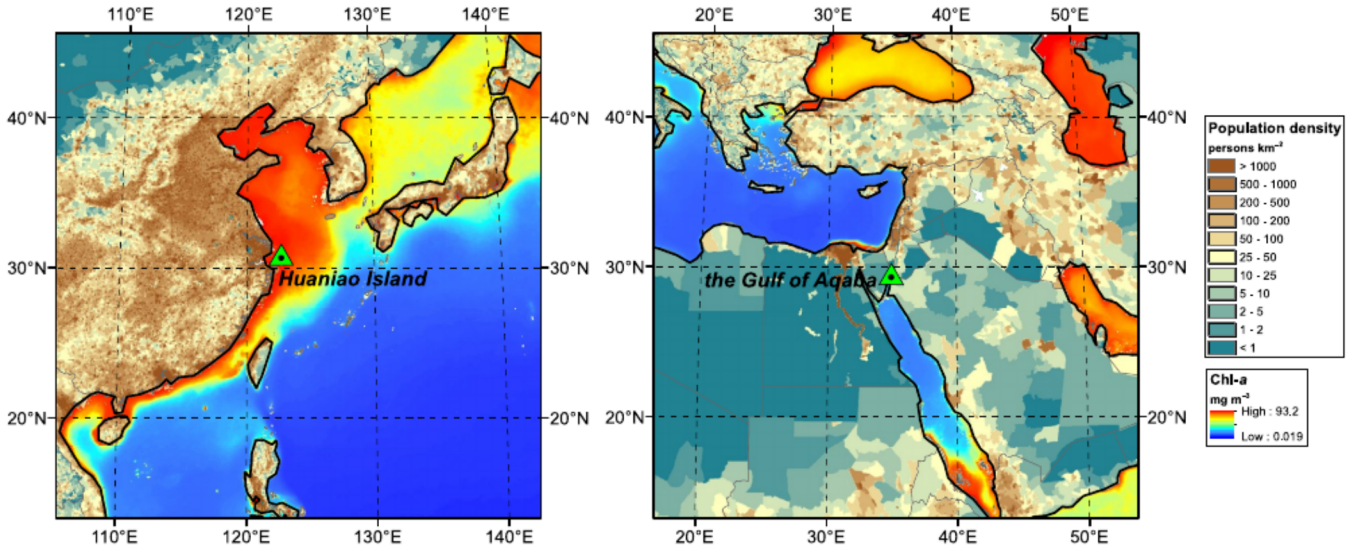

Figure 1. Locations of Huaniao Island and the Gulf of Aqaba (green triangles) with the background of spatial distribution of average chlorophyll *a* concentrations during 2000–2018 (Terra-MODIS) and population density in 2015 (gridded population of the world, version 4: Population density, revision 11) (Center for International Earth Science Information Network - CIESIN - Columbia University, 2018).

and chemical analysis were presented in previous studies (Chen et al., 2007; Wang et al., 2016). The mass concentration of nss-SO_4^{2-} ([nss-SO_4^{2-}]) was calculated using Na^+ as the indicator of sea salt aerosol ($\left[\text{nss} - SO_4^{2-}\right] = \left[SO_4^{2-}\right] - 0.251\left[Na^+\right]$) (Claeys et al., 2017).

Table 1
Sampling Periods and Number of Samples at HNI and the GA

Sampling site	Sampling period	Season	Number of samples
HNI	March 22 to April 19, 2013	Spring	19
	July 18 to August 11, 2013	Summer	24
	October 20 to November 13, 2013	Autumn	23
	December 22, 2013 to January 14, 2014	Winter	22
	December 28, 2014 to January 19, 2015	Winter	21
	March 29 to May 5, 2015	Spring	36
	August 4 to August 23, 2015	Summer	19
	October 21 to November 15, 2015	Autumn	25
	December 30, 2015 to January 19, 2016	Winter	20
	July 22 to August 17, 2016	Summer	26
	October 24 to December 1, 2016	Autumn	33
	March 11 to March 19, 2017	Spring	8
	June 21 to July 9, 2017	Early summer	18
	August 28 to September 12, 2017	Late summer	13
	January 2 to January 25, 2018	Winter	19
	April 2 to May 3, 2018	Spring	31
	October 25 to November 22, 2018	Autumn	28
The GA	August 20, 2003 to November 22, 2004	One-year period	60
	May 5 to September 11, 2005	Spring, summer	36

GA, Gulf of Aqaba; HNI, Huaniao Island.

2.2. Air Mass Backward Trajectories and Attribution of Air Mass Source Regions

Air mass backward trajectories were calculated using the National Oceanic and Atmospheric Administration (NOAA) Air Resources Laboratory's Hybrid Single-Particle Lagrangian Integrated Trajectories (HYSPLIT) model (https://ready.arl.noaa.gov/HYSPLIT.php) (Stein et al., 2015) with the starting height at 100 m and a total run time of 72 h. National Centers for Environmental Prediction (NCEP)'s Global Data Assimilation System (GDAS) Archive (1° × 1°) was used in the trajectory calculation for HNI (ftp://arlftp.arlhq.noaa.gov/pub/archives/gdas1). NCEP/National Center for Atmospheric Research (NCAR) Global Reanalysis Data Archive (2.5° × 2.5°) (ftp://ftp.arl.noaa.gov/pub/archives/reanalysis) were used for the GA because the time coverage of GDAS data set only date back to December 2004. There are a total of 73 endpoints (including the receptor site) with the interval of 1 h along the entire 72-h trajectory. The meteorological parameters including temperature, relative humidity (RH), boundary layer height (BLH) and wind speed at each endpoint were also extracted from GDAS data set. In order to determine the main source regions of air masses transported to HNI and the GA during the sampling periods, we counted the number of endpoints of all trajectories (released every 3 h) in each 0.2° × 0.2° grid cell in the areas adjacent to HNI (10–65°N, 75–145°E) and the GA (22–50°N, 10–45°E) and normalized the non-zero endpoint numbers for all grid cells. The higher density of trajectory endpoints indicates the higher frequency that air masses cross the region, which is very likely to be the main source region during the sampling period.

2.3. Retention of Air Masses Over Land and Within Marine Boundary Layer

In order to identify whether an air mass was mainly from oceanic or terrestrial region, the retention ratio of the air mass over land (R_L) was calculated by Equation 1.

$$R_L = \frac{\sum_{i=1}^{N_{\text{land}}} e^{-\frac{t_i}{72}}}{\sum_{i=1}^{N_{\text{total}}} e^{-\frac{t_i}{72}}} \quad (1)$$

where N_{total} is the total number of trajectory endpoints. N_{land} is the total number of trajectory endpoints located over land, while t_i is the backward tracking time with the unit of hour and $e^{-\frac{t_i}{72}}$ is the weighting factor related to tracking time as the diffusion of air mass and deposition of particles take place along the transport, hence the regions corresponding to longer backward tracking time have weaker influence on the receptor site than the nearby regions. As a result, the larger R_L value indicates that the air mass is more influenced by terrestrial transport and its source region is more likely to be on land. The schematic diagram of R_L calculation is shown in Figure S1 in the Supporting Information S1. Similar methods to characterize air mass source region have been used in other studies. For example, Willis et al. (2017) have used the FLEXPART-WRF model to calculate the average residence time of sampled air masses over open water prior to a sampling site in the Arctic. Similar method has also been used in calculating the percentage of time spent by trajectories over different surface types (land, marginal ice zone, compact sea-ice, and open ocean) in the Antarctic (Decesari et al., 2020).

When the air mass is above marine boundary layer (MBL), its connection to local sea surface processes, including marine biogenic emission and subsequent atmospheric reactions, may be significantly weaker. Here the retention ratio of an air mass within marine boundary layer (R_{MBL}) was calculated by Equation 2.

$$R_B = \frac{\sum_{i=1}^{N_{\text{below}}} e^{-\frac{t_i}{72}}}{\sum_{i=1}^{N_{\text{ocean}}} e^{-\frac{t_i}{72}}} \quad (2)$$

Here, N_{ocean} is the total number of trajectory endpoints located over the ocean (referred to marine endpoints). N_{below} is the number of marine endpoints with the heights below BLH (Figure S1 in the Supporting Information S1). $e^{-\frac{t_i}{72}}$ is the weighting factor related to tracking time. The larger R_{MBL} values indicate that the movement of air over the ocean are mainly confined within marine boundary layer.

2.4. The Calculation of Air Mass Exposure to Chl-*a*

An air mass exposure to Chl-*a* (AEC) index can represent the influence extent of marine biogenic emission on sampled air mass. It has been used to analyze the relationships between phytoplankton biomass and volatile organic compounds (VOCs) (Arnold et al., 2010), trace elements deposition (Blazina et al., 2017), and atmospheric DMS (Park et al., 2018) in various environments. This approach is based on a simple tenet that the emission of a biogenic compound should be positively related to the surface phytoplankton biomass in the surrounding area of air transport path. Although several studies have pointed out that Chl-*a* is not directly correlated with atmospheric components as plankton physiology or other physiochemical states of surface oceans control the production and emission of biogenic gases or aerosols (Quinn et al., 2014; Simo & Pedros-Alio, 1999), Chl-*a* is still a good proxy in this study because field observations revealed that seawater DMS concentrations usually highly correlated with Chl-*a* in coastal seas (Yang et al., 2011; Zhang et al., 2014). In addition to emission intensity, the BLH greatly affects the vertical convectional mixing and concentrations of atmospheric substances in boundary layer (Tang et al., 2016). Hence, in this study, we modified the calculation of AEC index on the basis of Park et al. (2018) by adding a term reciprocal to BLH. The AEC for each trajectory was calculated using Equation 3.

$$\mathrm{AEC} = \frac{\sum_{i=0}^{72} \mathrm{Chl}a_i \cdot e^{-\frac{t_i}{72}} \cdot \frac{600}{\mathrm{BLH}}}{n} \tag{3}$$

Here $\mathrm{Chl}a_i$ represents the mean Chl-*a* concentration within a radius of 20 km at a given endpoint (Figure S1 in the Supporting Information S1) from Terra-MODIS Chl-*a* concentration products (OCI algorithm, 8-day composite, 0.042° × 0.042°, https://oceandata.sci.gsfc.nasa.gov/MODIS-Terra/Mapped/8-Day/4km/chlor_a/). $\mathrm{Chl}a_i$ is set to zero if the endpoint locates on land or the air mass pressure is below 850 hPa. If no MODIS Chl-*a* concentrations are available at the endpoint over the ocean and with the pressure higher than 850 hPa, this endpoint will be excluded. t_i is the tracking time of endpoint. n is the total number of endpoints with valid Chl-*a* concentrations. The BLH below 50 m will be replaced by 50 m. In order to avoid the large uncertainty associated with large percentage of data missing, the AECs of trajectories with $n < 37$ were not calculated and set to invalid. $e^{-\frac{t_i}{72}}$ is the weighting factor related to tracking time. The AEC corresponding to each TSP sample was calculated as the arithmetic average of AECs of all trajectories during the sampling duration (released every 3 h). Considering the different time resolutions between MODIS Chl-*a* products (8 days) and calculated backward trajectories (3 h), we compared the AEC indices calculated using MODIS products with those calculated using Geostationary Ocean Color Imager (GOCI) Chl-*a* products binned to 1-day resolution (details shown in the Supporting Information S1). The AEC values based on the two satellite products agree quite well (Figure S2 in the Supporting Information S1), suggesting that using 8-day MODIS products is credible.

3. Results and Discussion

3.1. Concentrations and Seasonal Variations of MSA

Large seasonal and inter-annual variations of MSA and nss-SO_4^{2-} concentrations were observed over HNI. The highest seasonal average concentrations of MSA (0.067 μg m^{-3}) and nss-SO_4^{2-} (13.26 μg m^{-3}) occurred in the spring and winter of 2015, respectively, while the highest average MSA/nss-SO_4^{2-} (0.014) took place in the late summer of 2017 and spring of 2018 (Figure 2a). The average MSA concentration ([MSA]) during 2013–2018 over HNI (0.040 ± 0.034 μg m^{-3}) was in the same order of magnitude as those measured in the middle- and low-latitude open oceans, but the average [nss-SO_4^{2-}] (7.39 ± 5.43 μg m^{-3}) was an order of magnitude higher, which was only slightly lower than those of coastal cities in eastern China (Figure 2d and Table S1 in the Supporting Information S2). This gives a basic understanding that the atmospheric environment in the coastal ECS is significantly affected by the terrestrial transport of anthropogenic pollutants, which was consistent with a large part of the air mass source regions located on land (Figure 3). As for inter-annual variation, the average [nss-SO_4^{2-}] from 2013 to 2015 was 2.38 times as much as the average from 2016 to 2018. The sharp decline is likely to be resulted from China's effective pollution control and abatement in recent years, especially the obvious reduction of point source SO_2 emissions (van der A et al., 2017; Zheng et al., 2018). [MSA] also showed a decrease but the trend was milder, and the average

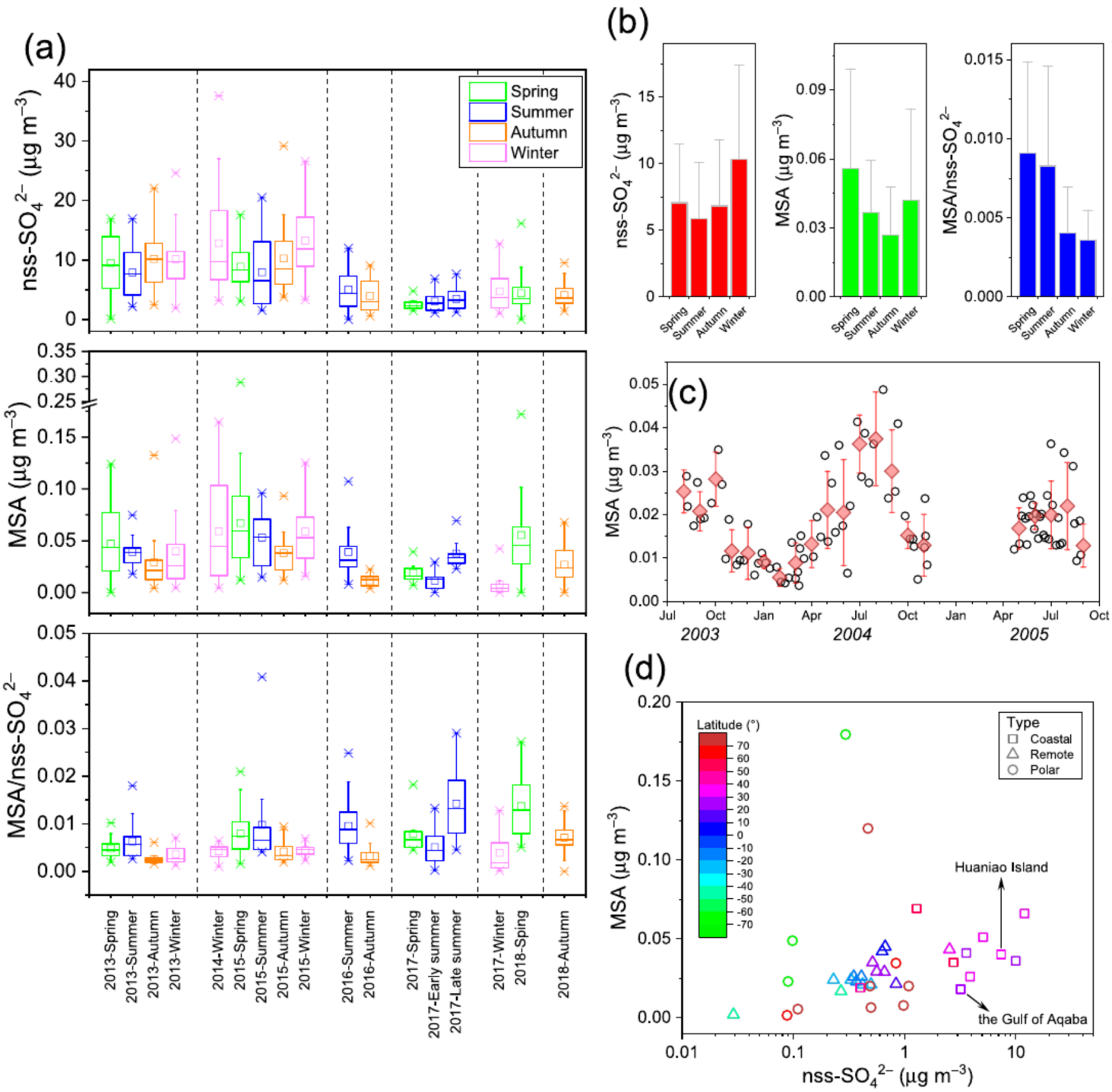

Figure 2. (a) Concentrations of methanesulfonate (MSA) and nss-SO_4^{2-} and ratios of MSA to nss-SO_4^{2-} (MSA/nss-SO_4^{2-}) over Huaniao Island (HNI) in each sampling season. The box chart demonstrates 25%–75% percentile with whiskers representing the range of outlier. Horizontal line in box represents the median. The meanings of other symbols are shown as below: "–" minimum and maximum; "×"1% and 99%; "□" mean. (b) Seasonal variations of MSA and nss-SO_4^{2-} concentrations as well as MSA/nss-SO_4^{2-} over HNI. (c) Time series of MSA concentration over the GA. The red diamond represents monthly mean and error bar represents standard deviation. (d) Comparison of average MSA and nss-SO_4^{2-} concentrations over HNI and the GA with those reported in previous studies. The detailed information of the data shown in this figure and literature sources are listed in Table S1 in the Supporting Information S2.

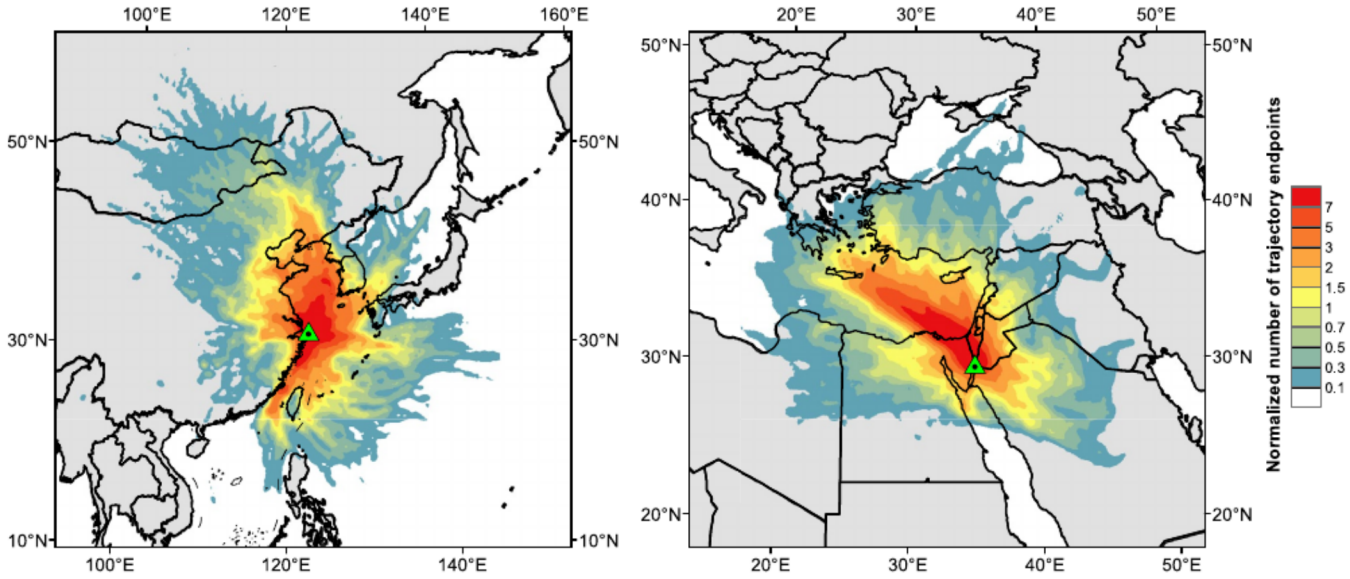

Figure 3. Spatial distributions of normalized numbers of air mass trajectory endpoints for Huaniao Island and the Gulf of Aqaba during the sampling periods, representing the distribution of main source regions for air masses transported to receptor sites.

ratio of MSA/nss-SO_4^{2-} during 2016–2018 was 1.36 times higher than that during 2013–2015. The average [MSA] (0.018 ± 0.010 μg m^{-3}) over the GA was much lower than that over HNI, corresponding to the relatively low ocean productivity. Although terrestrial transport also significantly influences the GA (Figure 3), the lower [nss-SO_4^{2-}] (3.20 ± 1.25 μg m^{-3}) than HNI suggested that anthropogenic emissions from surrounding land should be much lower than eastern China.

As shown in Figure 2b, [nss-SO_4^{2-}] was the highest in winter (10.33 ± 7.09 μg m^{-3}) and the lowest in summer (5.88 ± 4.19 μg m^{-3}). This is consistent with previous studies, and the higher pollutant emissions and prevailing northwesterly winds in winter result in the highest [nss-SO_4^{2-}] (Sun et al., 2015; Wang et al., 2015, 2016). [MSA] was the highest in spring (0.056 ± 0.043 μg m^{-3}), followed by winter (0.042 ± 0.040 μg m^{-3}), and the lowest in summer and autumn (0.037 ± 0.023 and 0.027 ± 0.021 μg m^{-3}, respectively). Differently, MSA/nss-SO_4^{2-} was much higher in spring and summer than in autumn and winter ($P < 0.001$). The seasonal variation of [MSA] is significantly different from those of other mid-latitude regions of the world. Observations in the Eastern Mediterranean from 1996 to 1999 showed that [MSA] was the highest in summer and the lowest in winter, which was consistent with the seasonal variation of DMS emission flux (Kouvarakis et al., 2002; Kouvarakis & Mihalopoulos, 2002; Kubilay et al., 2002). In addition, long-term observations in Cape Grim, Tasmania from 1988 to 1990 (Ayers et al., 1991), and Mace Head, Ireland from 1993 to 1994 (McArdle et al., 1998) also showed similar results. In surrounding marginal seas, seawater DMS concentration and DMS emission flux were found to be two to three times higher in summer than those in winter (Yang et al., 2011). The reason for mismatch between the seasonal variation of [MSA] and marine DMS emission needs to be carefully studied. In contrast, [MSA] over the GA exhibited a typical seasonal cycle like other mid-latitude oceans, which was the highest in summer and the lowest in winter (Figure 2c). Therefore, marine biogenic sulfur emission was likely an important factor controlling MSA over the GA.

The formation and loss of aerosol MSA are affected by many environmental factors. The oxidation of DMS involves both gas- (with OH, NO_3, reactive halogens, etc.) and aqueous-phase reactions (Hoffmann et al., 2016), and different reaction pathways will lead to different product structures. Recent studies have found that aqueous-phase oxidation is the main formation pathway of aerosol MSA (Hoffmann et al., 2016; Van Rooy et al., 2021; Zhu et al., 2006), and the cloud processing can greatly increase the yield of MSA. For example, significant positive relationship has been observed between [MSA] and particle liquid water content over the coastal city Hong Kong (Huang et al., 2015), and both [MSA] and MSA/nss-SO_4^{2-} have been found much higher in cloud water than in submicron particles over the coastal areas of western United Sates (Sorooshian et al., 2015). The mean RH along each trajectory was calculated and then averaged to each TSP sample (RH_traj). As shown in Figure 4a, the RH_traj over HNI was the highest in summer and the

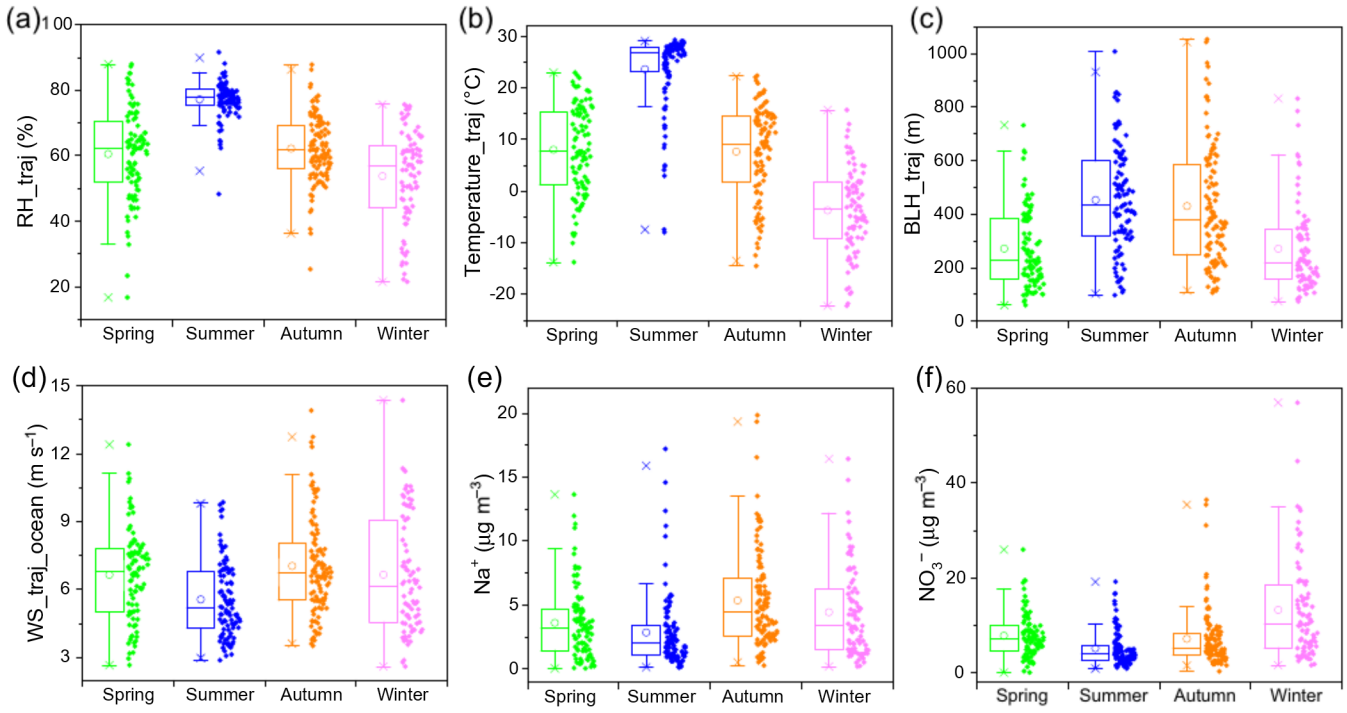

Figure 4. (a–d) Seasonal variations of averaged meteorological parameters along trajectories including (a) relative humidity, (b) temperature, (c) boundary layer height (harmonic mean) and (d) wind speed (along trajectories over oceanic region only) for each sample collected at Huaniao Island (HNI). (e and f) Seasonal variations of Na^+ and NO_3^- concentrations over HNI. The box chart demonstrates 25%–75% percentile with whiskers representing the range of outlier. The horizontal line and circle in box represent the median and mean respectively, and the markers "×" represent 1% and 99%.

lowest in winter with an average of 77.2% and 53.7%, respectively. Therefore, the intensity of aqueous-phase oxidation of DMS cannot explain the phenomenon of higher [MSA] in winter than in summer.

The initial reaction step of DMS with OH is a two-channel mechanism involving hydrogen abstraction and OH addition, and the latter channel will lead to a higher yield of MSA (Barnes et al., 2006; Bates et al., 1992). In ambient temperature range, the overall reaction rate coefficient for OH + DMS and the branching ratio of addition channel both increase with the decrease of temperature (Figure S4 in the Supporting Information S1) (Barnes et al., 2006; Gondwe et al., 2004; Hynes et al., 1986). Therefore, the amplification of addition channel and the subsequent higher yield ratio of OH initiated formation of MSA under low temperature conditions (Figure 4b) may be one of the reasons leading to higher [MSA] in winter than in summer over HNI. In addition, due to the potential oxidation loss of particulate MSA by OH radical (Kwong et al., 2018; Mungall et al., 2017), the higher concentration of atmospheric OH in summer may also cause lower [MSA].

Several previous studies have indicated that NO_3 radical is equally or even more important than OH in oxidizing DMS over coastal regions under the influence of anthropogenic NO_x. For example, the measurements off the New England Coast (the mean NO_2 concentration was 4 ppbv) demonstrated that there was an anticorrelation between NO_3 and DMS concentrations (Stark et al., 2007). A long-term observation on the north coast of Crete, eastern Mediterranean showed that the DMS oxidation by NO_3 was 2.7 and 8.5 times as effective as that by OH in summer and winter, respectively (Vrekoussis et al., 2006). Although NO_3 radical has not been directly measured, the concentration of NO_3^- over HNI were measured (Figure 4f) and NO_2 over adjacent monitoring stations (Dinghai, Putuo and Chuansha, Figures S5 and S6, in the Supporting Information S1) were obtained, and they all exhibited a significant seasonal cycle, that is, the highest in winter and the lowest in summer. Accordingly, the importance of NO_3 relative to OH oxidation may increase in winter like over the eastern Mediterranean. The dominantly initial step of gas-phase DMS + NO_3 reaction is hydrogen abstraction, which leads to a higher end-product yield of SO_4^{2-} than MSA (Barnes et al., 2006). Hence the gas-phase chemistry of DMS + NO_x/NO_3 may not be the cause of the abnormal seasonal variation of MSA over HNI.

Reactive halogens, such as BrO and Cl radicals, are also important DMS oxidants in MBL. But the modeling study has revealed that their contributions to DMS oxidation over coastal seas are likely to be insignificant, in competition with NO_3 and OH (Breider et al., 2010). Furthermore, the knowledge of reactive halogens over this region is still quite limited due to the lack of field observations and the strong influence of terrestrial sources (Peng et al., 2021; Wang et al., 2020). Hence the potential roles of reactive halogens in the MSA formation are not further discussed.

In addition to chemical processes, physical conditions may also greatly influence the MSA concentration in MBL, such as BLH controlling the dispersion of atmospheric constitutes (Li et al., 2017) and wind speed affecting the sea-to-air flux of DMS (Liss & Merlivat, 1986; Wanninkhof, 1992). As shown in Figure 4c, the average BLH along trajectories (BLH_traj, harmonic mean of BLH at each trajectory endpoints for a specific sample) was the lowest in winter (227 m), which was only about half of the average BLH_traj in summer (440 m) (Figure 4c). Besides, [MSA] and [nss-SO_4^{2-}] were found to be negatively correlated with BLH_traj (Figure S7 in the Supporting Information S1). This indicates that the weaker ventilation along air mass transport could elevate [MSA] in winter, and it further emphasizes the necessity of adding BLH into the AEC index calculation.

The seasonal averages of wind speed along marine trajectories (WS_traj_ocean) for HNI were 6.65, 5.56, 7.04 and 6.65 m s^{-1} in spring, summer, autumn and winter, respectively (Figure 4d). Similarly, the average concentration of sea-salt aerosols (proxied by Na^+) was also the highest in autumn and the lowest in summer (Figure 4e). In addition, [Na^+] was found to be significantly correlated with WS_traj_ocean ($r = 0.72$), but its correlation with the local wind speed at HNI was much weaker ($r = 0.43$) (Figure S8 in the Supporting Information S1). This suggested that the WS_traj_ocean was a better index of marine primary emission than local wind speed at the receptor site. By contrast, there was no correlation between [MSA] and WS_traj_ocean at HNI (Figure S8 in the Supporting Information S1). Similarly, no seasonal covariation was found between the above two variables at the GA (Figure S3 in the Supporting Information S1). Thus, wind speed was not a primary factor causing the seasonal variation of MSA though it could greatly influence the emission of oceanic DMS.

3.2. Dominant Source Regions of MSA in Different Seasons

The above section discussed several possible reasons of the abnormal seasonal variation of MSA at HNI, but it cannot clarify whether wintertime MSA was derived from marine sources. The R_L reflects the influence of terrestrial sources on aerosol composition. In HNI, the R_L values corresponding to summer samples were mostly distributed at low levels with 38.0% equal to zero and 76.0% lower than 0.1 (Figure 5a). By contrast, the R_L values in winter were much higher, of which 43.9% were greater than 0.5. Moderate R_L values were found in spring and autumn with the average R_L higher in autumn (0.33) than in spring (0.24). The seasonal pattern of R_L values reveals the increasing influence of terrestrial transport on the coastal ECS from summer to winter, under the transition of prevailing wind directions of East Asia Monsoon. When selecting samples mainly from the ocean with little perturbation by terrestrial sources ($R_L < 0.1$), [MSA] showed a seasonal variation as spring > summer > autumn > winter (Figure 5b). Therefore, the high concentrations of wintertime MSA were very likely not to be contributed by marine sources.

It should be noted that MSA is mostly distributed in fine particles with a lifetime of several days (Jung et al., 2014; Kerminen et al., 1997; Sorooshian et al., 2015), and therefore it is reasonable to relate the MSA concentrations measured in TSP with the indexes calculated on the basis of 72-h trajectories of air masses. As shown in Figure 6, negative correlations between MSA/nss-SO_4^{2-} and R_L were observed in spring and summer, consistent with the general understanding that MSA is mainly from the ocean while nss-SO_4^{2-} is mainly from the terrestrial anthropogenic sources. In autumn, there was no obvious correlation between these two variables. Unexpectedly, there was a significant positive correlation between MSA/nss-SO_4^{2-} and R_L in winter, which meant the value of MSA/nss-SO_4^{2-} was higher in air masses originating from the land than from the ocean. The intercept of linear fitting for wintertime data is 0.00138 ± 0.00046. If we use this value as the end member value of marine air masses, we can approximate the concentration of marine MSA by multiplying [nss-SO_4^{2-}] by this value. As a result, the average concentration of marine MSA in winter was 0.014 ± 0.005 μg m^{-3}, accounting for only 34.0 ± 11.3% of total MSA (more than half from terrestrial sources). Considering the deposition of marine MSA during transport and the higher concentration of nss-SO_4^{2-}

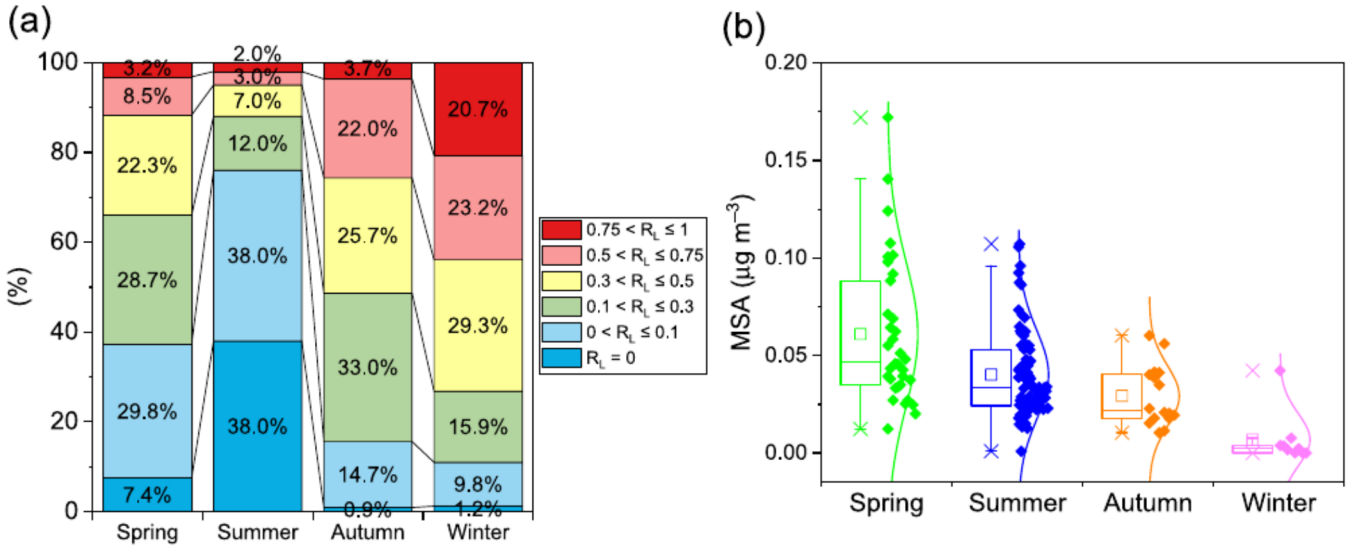

Figure 5. (a) The proportions of different R_L ranges for samples collected in different seasons over Huaniao Island (HNI). (b) [MSA] in different seasons over HNI with the airmasses transported mainly from the ocean ($R_L < 0.1$). The box chart demonstrates 25%–75% percentile with whiskers representing the range of outlier. The horizontal line and square in box represent the median and mean respectively, and the markers "×" represent 1% and 99%.

over the land than that over the sea, the ratio of marine MSA to nss-SO_4^{2-} was lower than 0.00138 ± 0.00046 when affected by terrestrial air masses. Therefore, the actual marine biogenic contribution to aerosol MSA was likely to be even lower than abovementioned estimation. This phenomenon suggested that wintertime MSA over HNI could be strongly contributed by terrestrial sources from eastern China. While in spring and summer, MSA was predominantly from the ocean; and in autumn, it could be derived from the mixture of both terrestrial and marine sources. As for the GA, a significantly negative correlation was found between MSA/nss-SO_4^{2-} and R_L (Figure S9 in the Supporting Information S1), suggesting that aerosol MSA was predominantly derived from marine sources in accordance with its annual cycle.

3.3. Linkage to Marine Phytoplankton Biomass

AEC can serve as an indicator of the strength of marine biogenic sources affecting the components in atmospheric aerosols. In general, the AEC at HNI is significantly higher in spring and summer than in other two seasons (Figures S10 and S11 in the Supporting Information S1). The average values in four seasons are: 2.78 ± 4.53 mg m^{-3} in spring, 1.77 ± 1.86 mg m^{-3} in summer, 0.45 ± 0.33 mg m^{-3} in autumn, and 0.43 ± 0.66 mg m^{-3} in winter. Extremely high AEC values (>10 mg m^{-3}) occurred in the spring of 2015 and early summer of 2017 with low R_L (< 0.1). The seasonal variation of AEC is in accordance with that of [MSA] in the samples corresponding to air masses mainly from the ocean (Figure 5b).

The correlations between [MSA] and AEC under different conditions were investigated. As shown in Figure 7a, R_L significantly affected their correlations in HNI, and high correlation coefficients were found under extremely low level of R_L. This indicated that MSA was linked to marine biogenic sources when air masses were solely transported from the ocean. Significant contribution of terrestrial sources could interfere with the linkage between MSA and marine productivity. As for the GA, R_L showed little effect on the correlation coefficients between [MSA] and AEC (Figure 7b), implying that land source contribution to MSA was negligible.

In addition to the effect of R_L, the correlations between [MSA] and AEC for both HNI and the GA could be enhanced by applying R_{MBL} filtration to high levels, especially for $R_{MBL} > 0.9$ (Figure 7). This suggested that ocean surface emissions had a strong influence on the local chemical composition of aerosols within marine boundary layer, but not on those above boundary layer. It highlights the importance of air transport height in linking the atmospheric components with surface sources along the transport path. Only when marine air mass transport mainly within boundary layer can the valid linkage be established. Therefore, the application of spatiotemporal correlation analysis, potential source contribution function (PSCF), or concentration

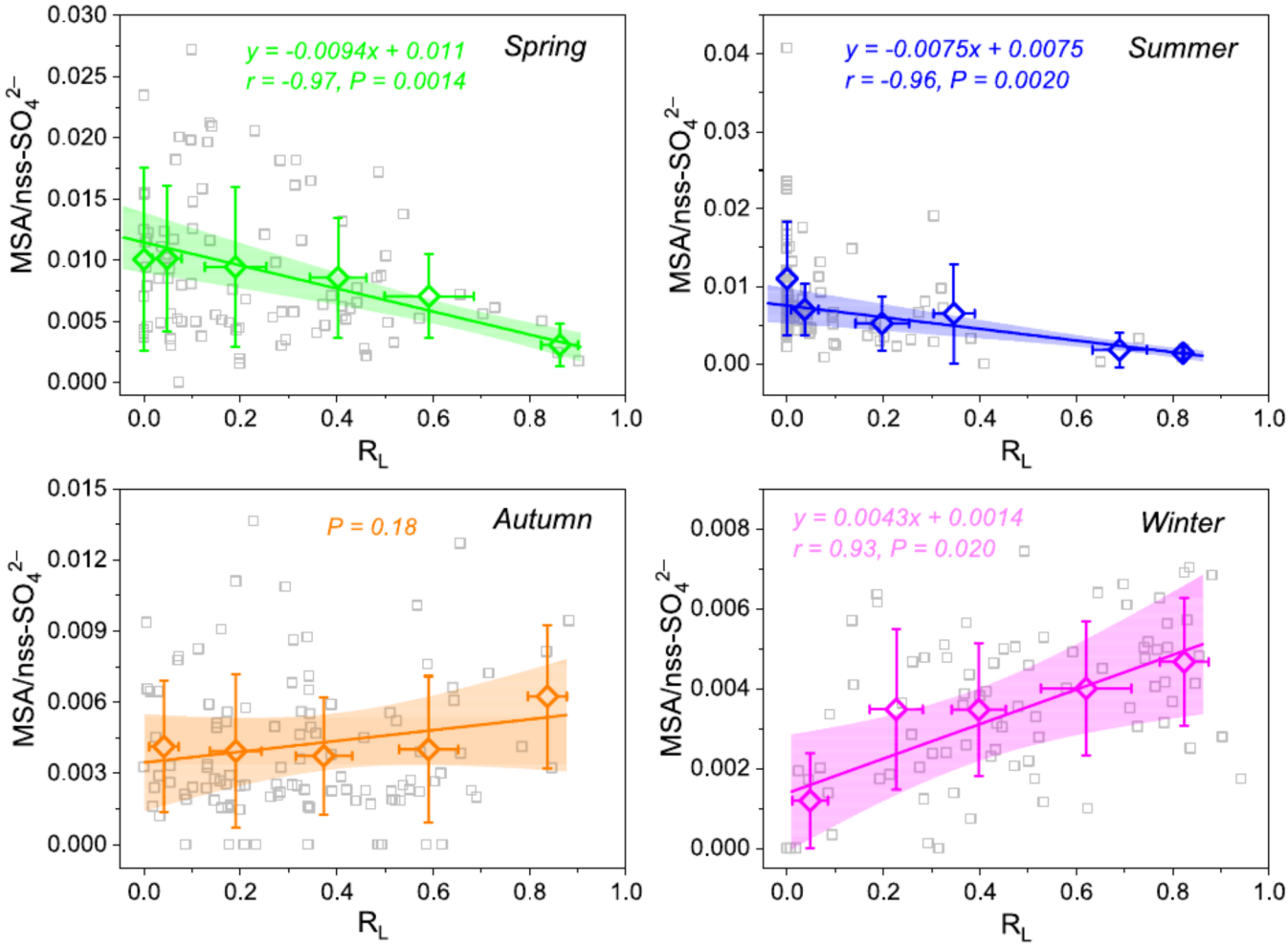

Figure 6. Relationships between the ratio of methanesulfonate to nss-SO_4^{2-} and R_L in different seasons over Huaniao Island. The gray open dots represent the raw data, and the colored diamonds with error bars represent the binned data according to the R_L ranges in Figure 5a and their standard deviations. As for autumn and winter, because there is only one data corresponding to $R_L = 0$, this data is binned into the second range ($0 < R_L \leq 0.1$). The lines and shaded regions show the linear regressions for binned data and their 95% confidence intervals.

weighted trajectories (CWTs) without considering R_{MBL} (Mansour et al., 2020; Stahl et al., 2020) may cause biases in identifying MSA source regions. As for HNI, it should be noted that the correlation did not improve with the filtration of R_{MBL} to higher level when $R_{MBL} > 0.6$ under the condition of $R_L = 0$. This is because most of the data under the condition of $R_{MBL} > 0.6$ are already in the range of $R_{MBL} > 0.9$ (37 of 43, Figure S12 in the Supporting Information S1).

Under the condition of $R_{MBL} > 0.9$, significantly positive correlations between [MSA] and AEC were found in spring and summer over HNI (Figure 7c), whereas no correlations existed in autumn and winter. As for the GA, [MSA] was positively correlated with AEC for the two-year sampling period (Figure 7d). In conclusion, the contribution of non-marine sources to aerosol MSA was insignificant in the GA and in the spring and summer of coastal ECS, and in these situations MSA could be used as a good indicator for biological influence.

3.4. Potential Terrestrial Sources

Industrial emissions and biomass burning are two important sources of atmospheric pollutants over eastern China (Bi et al., 2019; Wang et al., 2005) and are likely to emit abundant MSA precursors as mentioned above. Unfortunately, there is little information about the emission factor for volatile organic sulfur

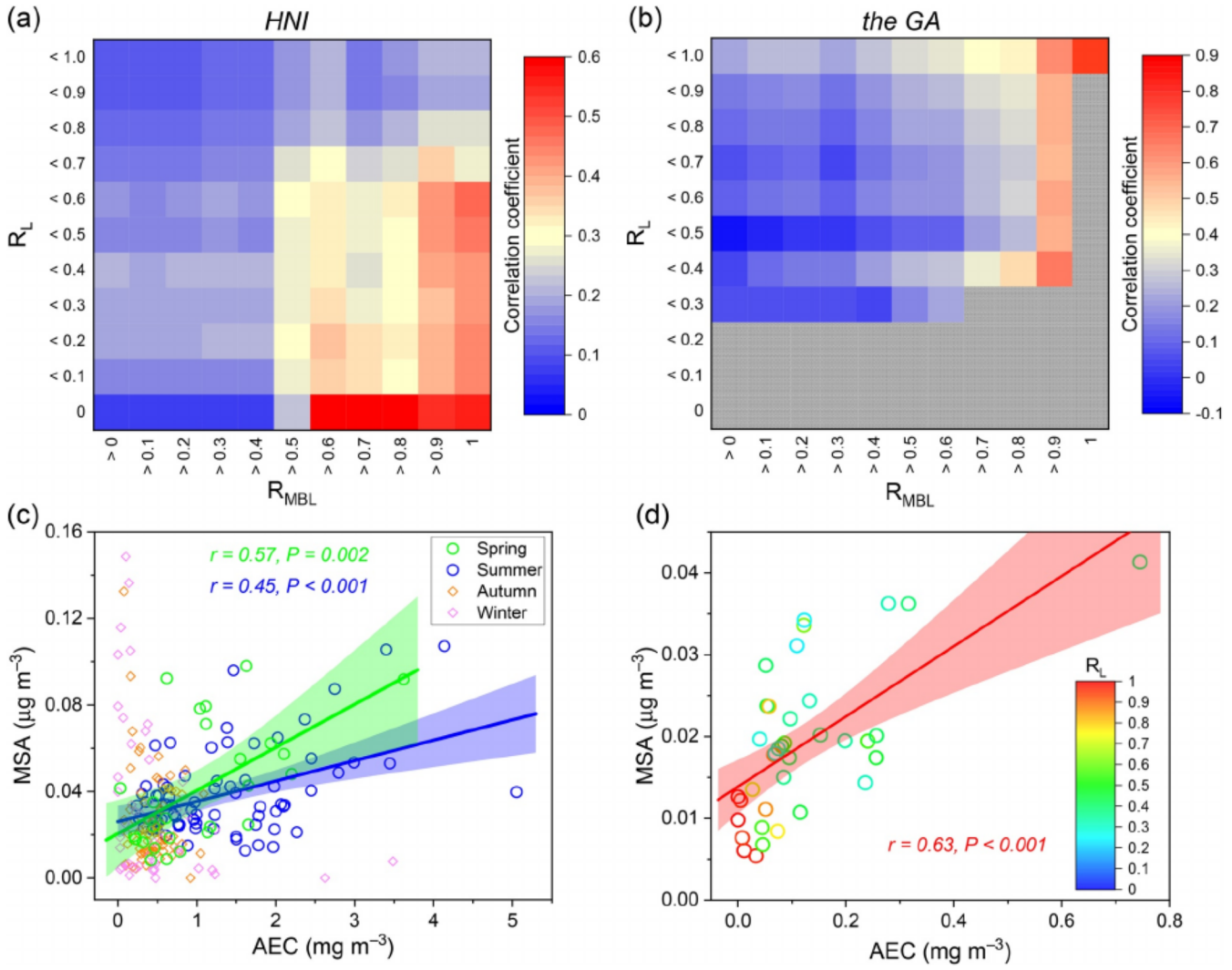

Figure 7. Correlation coefficient (Pearson's) matrix of [MSA] and air mass exposure to Chl-*a* (AEC) in different R_L and R_{MBL} ranges for (a) Huaniao Island (HNI) and (b) the Gulf of Aqaba (GA). The gray grids represent that the valid data numbers are less than nine. The number of data points for each grid is shown in Figure S12 in the Supporting Information S1. The scatter plots show the relationships between [MSA] and AEC when marine air masses were mainly under the boundary layer ($R_{MBL} > 0.9$) in different seasons for (c) HNI and (d) the GA. The lines and shaded regions show the linear regressions and 95% confidence intervals.

compounds from these sources. Therefore, it is difficult to estimate their emissions and relative contribution to sulfur components in regional atmosphere.

Non-marine biogenic sources may be another important contributor to MSA precursors in eastern China. For example, some higher plants in salt marshes, especially *Spartina alterniflora*, can also emit a large amount of DMS (Dacey et al., 1987; De Mello et al., 1987). *Spartina alterniflora* is the main invasive plant along the coastal wetlands of China. The total area covered by this species is 34,178 ha in China in 2006–2008 and 94.22% of the area locates in eastern Jiangsu Province, Shanghai, and Zhejiang Province surrounding HNI (Lu & Zhang, 2013). A field measurement conducted in a salt marsh in Jiangsu has found that the emission flux of DMS by *Spartina alterniflora* is much higher in winter (297.0 ± 24.8 μgS m^{-2} h^{-1}) than in other seasons, resulting from higher DMSP lyase activity in senescing tissue in winter (Wang & Wang, 2017). This flux value is about 32–70 times the average sea-to-air flux of DMS from the ECS and the Yellow Sea (YS) (4.25–9.32 μgS m^{-2} h^{-1}) measured in January to February, 2007 (Yang et al., 2011). Therefore, the contribution of DMS emitted by *Spartina alterniflora* is nonnegligible, especially for offshore areas close to coastal wetlands like HNI. In addition, a recent study pointed out that DMS is also ubiquitous in freshwater lakes

in eastern plain of China, with the concentration ranging from 7.8–694 ng L^{-1} (Deng et al., 2020). DMS can also originate from paddy soil by anaerobic microorganism degradation and the emission will be higher when organic manure and chemical fertilizer are both applied (Yang et al., 1996).

In conclusion, there are significant emissions of MSA precursors from both anthropogenic and natural sources in eastern China. Together with high DMS-to-MSA yield ratio under low temperature and weak ventilation under low BLH in winter, abundant aerosol MSA is formed and then transported to marginal seas by East Asian winter monsoon, which makes a dominant contribution to MSA in marine aerosols. The results highlight the need to characterize MSA precursor emissions from terrestrial environments, their distributions, seasonalities, and their impacts on marine aerosol physicochemical properties. The significant contribution of terrestrial sources to MSA could also explain the slight inter-annual decreasing trend of MSA over HNI as shown in Figure 2a. With the on-going air pollution control, the anthropogenically derived MSA may have been decreasing like nss-SO_4^{2-}, but the amount of MSA derived from natural sources may remain stable. Therefore, the overall MSA exhibited a decrease during 2013–2018, but the decreasing trend was slighter than nss-SO_4^{2-}. Correspondingly, the ratios of MSA to nss-SO_4^{2-} showed an increasing trend. In the future, with the further decline of anthropogenic air pollutants in China, natural components originating from both marine and terrestrial biogenic sources will play more and more important roles in the atmospheric chemistry. As for the GA, the relatively low population density, extremely arid climate, low intensity of agricultural activity, and lack of lakes and coastal wetlands in its surrounding continent result in that terrestrial DMS emissions from both anthropogenic and natural sources are negligible.

4. Conclusions

We obtained long-term observational data of MSA and nss-SO_4^{2-} in aerosols over two distinct coastal sites. MSA over the GA, surrounded by arid land with low vegetation coverage and population density, exhibited a typical seasonal cycle as mid-latitude oceans (highest in summer and lowest in winter). Although the emission of DMS from adjacent marginal seas is much higher in summer than that in winter (Yang et al., 2011), MSA concentration over HNI was higher in winter. The accumulation of aerosols under low boundary layer and high conversion rate of DMS to MSA under low temperature conditions may play roles in causing this abnormal seasonal variation, but they cannot clarify where the wintertime MSA originated. By analyzing the relationships between MSA, nss-SO_4^{2-}, and R_L, we found that ocean-derived MSA contributed less than 34.0% of total MSA over HNI in winter. Therefore, MSA precursors from terrestrial sources, including both anthropogenic and natural emissions, were the dominant contributors to wintertime MSA. Due to the substantial influences of terrestrial MSA sources, the correlation between MSA and AEC was greatly affected by the level of R_L. This phenomenon was absent in the GA, suggesting that there was no terrestrial MSA sources around it. In addition, we found that the linkage between MSA and phytoplankton biomass was valid only when air masses were mainly constrained within MBL. By applying the filtration of R_{MBL} to greater than 0.9, MSA was significantly correlated with AEC in spring and summer over HNI, but not in autumn and winter. Therefore, in the spring and summer of coastal ECS, MSA is still predominantly derived from marine biogenic sources and can serve as a qualitative indicator for marine biological influence.

In conclusion, air mass history needs to be carefully considered when using MSA as an indicator for marine biogenic sources in coastal seas especially near urban/industrial centers or certain biogeographic zones with great emission flux of MSA precursors. Good correlations between atmospheric MSA and surface phytoplankton biomass were established by filtration for clean marine air masses and confining the air transport within marine boundary layer. This approach can be used to link other marine biogenic compounds in the atmosphere (like amines (Zhou et al., 2019), hydrocarbons, and other secondary and primary organic compounds (Gantt & Meskhidze, 2013; Palmer & Shaw, 2005)) to sea surface phytoplankton, which is very useful for construct parameterizations to obtain their spatiotemporal distributions using satellite ocean color datasets.

Data Availability Statement

All field observation data used in this study and calculated indices as well as Matlab codes to calculate them are available at http://dx.doi.org/10.17632/w4rj7jrfkt.1. The GDAS meteorological data set can be accessed at ftp://ftp.arl.noaa.gov/pub/archives/gdas1. The remote-sensing Chl-*a* datasets are available at https://oceandata.sci.gsfc.nasa.gov/. The NCEP/NCAR's Global Reanalysis Data can be accessed at ftp://ftp.arl.noaa.gov/pub/archives/reanalysis.

Acknowledgments
This work is jointly supported by the National Key Research and Development Program of China (2016YFA0601304), the National Natural Science Foundation of China (41775145), and the National Key Basic Research Program of China (2014CB953701). We gratefully acknowledge the NOAA Air Resources Laboratory for providing the HYSPLIT model, and NASA's OceanColor Web for the distribution of MODIS and GOCI data set. We are sincerely grateful to Yueping Chen and Yaping Zhang for their sampling assistance on Huaniao Island. Shengqian Zhou acknowledges Fujiang Wang, Bo Wang, Xiaofei Qin, Tianfeng Guo, and Hao Li for their assistance with field and laboratory work.

References

Arnold, S. R., Spracklen, D. V., Gebhardt, S., Custer, T., Williams, J., Peeken, I., & Alvain, S. (2010). Relationships between atmospheric organic compounds and air-mass exposure to marine biology. *Environmental Chemistry*, *7*(3), 232. https://doi.org/10.1071/en09144

Ayers, G., Ivey, J., & Gillett, R. (1991). Coherence between seasonal cycles of dimethyl sulphide, methanesulphonate and sulphate in marine air. *Nature*, *349*(6308), 404–406. https://doi.org/10.1038/349404a0

Barnes, I., Hjorth, J., & Mihalopoulos, N. (2006). Dimethyl sulfide and dimethyl sulfoxide and their oxidation in the atmosphere. *Chemical Reviews*, *106*(3), 940–975. https://doi.org/10.1021/cr020529+

Bates, T. S., Calhoun, J. A., & Quinn, P. K. (1992). Variations in the methanesulfonate to sulfate molar ratio in submicrometer marine aerosol-particles over the South-Pacific Ocean. *Journal of Geophysical Research*, *97*(D9), 9859–9865. https://doi.org/10.1029/92JD00411

Bi, X., Dai, Q., Wu, J., Zhang, Q., Zhang, W., Luo, R., et al. (2019). Characteristics of the main primary source profiles of particulate matter across China from 1987 to 2017. *Atmospheric Chemistry and Physics*, *19*(5), 3223–3243. https://doi.org/10.5194/acp-19-3223-2019

Blazina, T., Laderach, A., Jones, G. D., Sodemann, H., Wernli, H., Kirchner, J. W., & Winkel, L. H. (2017). Marine primary productivity as a potential indirect source of selenium and other trace elements in atmospheric deposition. *Environmental Science & Technology*, *51*(1), 108–118. https://doi.org/10.1021/acs.est.6b03063

Bork, N., Elm, J., Olenius, T., & Vehkamäki, H. (2014). Methane sulfonic acid-enhanced formation of molecular clusters of sulfuric acid and dimethyl amine. *Atmospheric Chemistry and Physics*, *14*(22), 12023–12030. https://doi.org/10.5194/acp-14-12023-2014

Breider, T. J., Chipperfield, M. P., Richards, N. A. D., Carslaw, K. S., Mann, G. W., & Spracklen, D. V. (2010). Impact of BrO on dimethylsulfide in the remote marine boundary layer. *Geophysical Research Letters*, *37*(2), L02807. https://doi.org/10.1029/2009gl040868

Bullock, H. A., Luo, H., & Whitman, W. B. (2017). Evolution of dimethylsulfoniopropionate metabolism in marine phytoplankton and bacteria. *Frontiers in Microbiology*, *8*, 637. https://doi.org/10.3389/fmicb.2017.00637

Carpenter, L. J., Archer, S. D., & Beale, R. (2012). Ocean-atmosphere trace gas exchange. *Chemical Society Reviews*, *41*(19), 6473–6506. https://doi.org/10.1039/c2cs35121h

Center for International Earth Science Information Network - CIESIN - Columbia University (2018). *Gridded population of the world, version 4 (GPWv4): Population density, revision 11*. NASA Socioeconomic Data and Applications Center (SEDAC).

Charlson, R. J., Lovelock, J. E., Andreaei, M. O., & Warren, S. G. (1987). Oceanic phytoplankton, atmospheric sulphur, cloud albedo and climate. *Nature*, *326*(6114), 655–661. https://doi.org/10.1038/326655a0

Chen, Y., Mills, S., Street, J., Golan, D., Post, A., Jacobson, M., & Paytan, A. (2007). Estimates of atmospheric dry deposition and associated input of nutrients to Gulf of Aqaba seawater. *Journal of Geophysical Research*, *112*(D4), 14. https://doi.org/10.1029/2006jd007858

Claeys, M., Roberts, G., Mallet, M., Arndt, J., Sellegri, K., Sciare, J., et al. (2017). Optical, physical and chemical properties of aerosols transported to a coastal site in the western Mediterranean: A focus on primary marine aerosols. *Atmospheric Chemistry and Physics*, *17*(12), 7891–7915. https://doi.org/10.5194/acp-17-7891-2017

Dacey, J. W. H., King, G. M., & Wakeham, S. G. (1987). Factors controlling emission of dimethylsulphide from salt marshes. *Nature*, *330*(6149), 643–645. https://doi.org/10.1038/330643a0

De Mello, W. Z., Cooper, D. J., Cooper, W. J., Saltzman, E. S., Zika, R. G., Savoie, D. L., & Prospero, J. M. (1967). Spatial and diel variability in the emissions of some biogenic sulfur compounds from a Florida *Spartinaalterniflora* coastal zone. *Atmospheric Environment*, *21*(4), 987–990. https://doi.org/10.1016/0004-6981(87)90095-3

Decesari, S., Paglione, M., Rinaldi, M., Dall'Osto, M., Simó, R., Zanca, N., et al. (2020). Shipborne measurements of Antarctic submicron organic aerosols: An NMR perspective linking multiple sources and bioregions. *Atmospheric Chemistry and Physics*, *20*(7), 4193–4207. https://doi.org/10.5194/acp-20-4193-2020

Deng, X., Chen, J., Hansson, L.-A., Zhao, X., & Xie, P. (2020). Eco-chemical mechanisms govern phytoplankton emissions of dimethylsulfide in global surface waters. *National Science Review*, *8*, nwaa140. https://doi.org/10.1093/nsr/nwaa140

Facchini, M. C., Decesari, S., Rinaldi, M., Carbone, C., Finessi, E., Mircea, M., et al. (2008). Important source of marine secondary organic aerosol from biogenic amines. *Environmental Science & Technology*, *42*(24), 9116–9121. https://doi.org/10.1021/es8018385

Gantt, B., & Meskhidze, N. (2013). The physical and chemical characteristics of marine primary organic aerosol: A review. *Atmospheric Chemistry and Physics*, *13*(8), 3979–3996. https://doi.org/10.5194/acp-13-3979-2013

Gao, Y., Arimoto, R., Duce, R. A., Chen, L. Q., Zhou, M. Y., & Gu, D. Y. (1996). Atmospheric non-sea-salt sulfate, nitrate and methanesulfonate over the China Sea. *Journal of Geophysical Research*, *101*(D7), 12601–12611. https://doi.org/10.1029/96jd00866

Gaston, C. J., Pratt, K. A., Qin, X., & Prather, K. A. (2010). Real-Time detection and mixing state of methanesulfonate in single particles at an inland urban location during a phytoplankton bloom. *Environmental Science & Technology*, *44*(5), 1566–1572. https://doi.org/10.1021/es902069d

Giri, B. S., Goswami, M., Pandey, R. A., & Kim, K. H. (2015). Kinetics and biofiltration of dimethyl sulfide emitted from P&P industry. *Biochemical Engineering Journal*, *102*, 108–114. https://doi.org/10.1016/j.bej.2015.02.038

Gondwe, M., Krol, M., Klaassen, W., Gieskes, W., & de Baar, H. (2004). Comparison of modeled versus measured MSA:nss $SO_4^=$ratios: A global analysis. *Global Biogeochemical Cycles*, *18*(2), GB2006. https://doi.org/10.1029/2003gb002144

Hodshire, A. L., Campuzano-Jost, P., Kodros, J. K., Croft, B., Nault, B. A., Schroder, J. C., et al. (2019). The potential role of methanesulfonic acid (MSA) in aerosol formation and growth and the associated radiative forcings. *Atmospheric Chemistry and Physics*, *19*(5), 3137–3160. https://doi.org/10.5194/acp-19-3137-2019

Hoffmann, E. H., Tilgner, A., Schroedner, R., Bräuer, P., Wolke, R., & Herrmann, H. (2016). An advanced modeling study on the impacts and atmospheric implications of multiphase dimethyl sulfide chemistry. *Proceedings of the National Academy of Sciences of the United States of America*, *113*(42), 11776–11781. https://doi.org/10.1073/pnas.1606320113

Huang, D. D., Li, Y. J., Lee, B. P., & Chan, C. K. (2015). Analysis of organic sulfur compounds in atmospheric aerosols at the HKUST supersite in Hong Kong using HR-ToF-AMS. *Environmental Science & Technology*, *49*(6), 3672–3679. https://doi.org/10.1021/es5056269

Hynes, A. J., Wine, P., & Semmes, D. (1986). Kinetics and mechanism of hydroxyl reactions with organic sulfides. *Journal of Physical Chemistry*, *90*(17), 4148–4156. https://doi.org/10.1021/j100408a062

Jung, J., Furutani, H., Uematsu, M., & Park, J. (2014). Distributions of atmospheric non-sea-salt sulfate and methanesulfonic acid over the Pacific Ocean between 48°N and 55°S during summer. *Atmospheric Environment*, *99*, 374–384. https://doi.org/10.1016/j.atmosenv.2014.10.009

Kerminen, V.-M., Aurela, M., Hillamo, R. E., & Virkkula, A. (1997). Formation of particulate MSA: Deductions from size distribution measurements in the Finnish Arctic. *Tellus B: Chemical and Physical Meteorology*, *49*(2), 159–171. https://doi.org/10.1034/j.1600-0889.49.issue2.4.x

Kouvarakis, G., Bardouki, H., & Mihalopoulos, N. (2002). Sulfur budget above the Eastern Mediterranean: Relative contribution of anthropogenic and biogenic sources. *Tellus B: Chemical and Physical Meteorology*, *54*(3), 201–212. https://doi.org/10.3402/tellusb.v54i3.16661

Kouvarakis, G., & Mihalopoulos, N. (2002). Seasonal variation of dimethylsulfide in the gas phase and of methanesulfonate and non-sea-salt sulfate in the aerosols phase in the Eastern Mediterranean atmosphere. *Atmospheric Environment*, *36*(6), 929–938. https://doi.org/10.1016/S1352-2310(01)00511-8

Kubilay, N., Koçak, M., Çokacar, T., Oguz, T., Kouvarakis, G., & Mihalopoulos, N. (2002). Influence of Black Sea and local biogenic activity on the seasonal variation of aerosol sulfur species in the eastern Mediterranean atmosphere. *Global Biogeochemical Cycles*, *16*(4), 27–12715. https://doi.org/10.1029/2002gb001880

Kwong, K. C., Chim, M. M., Hoffmann, E. H., Tilgner, A., Herrmann, H., Davies, J. F., et al. (2018). Chemical transformation of methanesulfonic acid and sodium methanesulfonate through heterogeneous OH oxidation. *ACS Earth and Space Chemistry*, *2*(9), 895–903. https://doi.org/10.1021/acsearthspacechem.8b00072

Lee, C.-L., & Brimblecombe, P. (2016). Anthropogenic contributions to global carbonyl sulfide, carbon disulfide and organosulfides fluxes. *Earth-Science Reviews*, *160*, 1–18. https://doi.org/10.1016/j.earscirev.2016.06.005

Li, Y., Wang, N., Barbante, C., Kang, S., Niu, H., Wu, X., et al. (2021). Spatial distribution and potential sources of methanesulfonic acid in high Asia glaciers. *Atmospheric Research*, *248*, 105227. https://doi.org/10.1016/j.atmosres.2020.105227

Li, Z., Guo, J., Ding, A., Liao, H., Liu, J., Sun, Y., et al. (2017). Aerosol and boundary-layer interactions and impact on air quality. *National Science Review*, *4*(6), 810–833. https://doi.org/10.1093/nsr/nwx117

Liss, P. S., & Merlivat, L. (1986). Air-sea gas exchange rates: Introduction and synthesis. In The role of air-sea exchange in geochemical cycling (Vol. 185, pp. 113–127). https://doi.org/10.1007/978-94-009-4738-2_5

Lu, J., & Zhang, Y. (2013). Spatial distribution of an invasive plant Spartina alterniflora and its potential as biofuels in China. *Ecological Engineering*, *52*, 175–181. https://doi.org/10.1016/j.ecoleng.2012.12.107

Mansour, K., Decesari, S., Bellacicco, M., Marullo, S., Santoleri, R., Bonasoni, P., et al. (2020). Particulate methanesulfonic acid over the central Mediterranean Sea: Source region identification and relationship with phytoplankton activity. *Atmospheric Research*, *237*, 104837. https://doi.org/10.1016/j.atmosres.2019.104837

McArdle, N., Liss, P., & Dennis, P. (1998). An isotopic study of atmospheric sulphur at three sites in Wales and at Mace Head, Eire. *Journal of Geophysical Research*, *103*(D23), 31079–31094. https://doi.org/10.1029/98JD01664

Meinardi, S. (2003). Dimethyl disulfide (DMDS) and dimethyl sulfide (DMS) emissions from biomass burning in Australia. *Geophysical Research Letters*, *30*(9), 1454. https://doi.org/10.1029/2003gl016967

Mihalopoulos, N., Kerminen, V. M., Kanakidou, M., Berresheim, H., & Sciare, J. (2007). Formation of particulate sulfur species (sulfate and methanesulfonate) during summer over the Eastern Mediterranean: A modelling approach. *Atmospheric Environment*, *41*(32), 6860–6871. https://doi.org/10.1016/j.atmosenv.2007.04.039

Mungall, E. L., Wong, J. P. S., & Abbatt, J. P. D. (2017). Heterogeneous oxidation of particulate methanesulfonic acid by the hydroxyl radical: Kinetics and atmospheric implications. *ACS Earth and Space Chemistry*, *2*(1), 48–55. https://doi.org/10.1021/acsearthspacechem.7b00114

Nakamura, T., Matsumoto, K., & Uematsu, M. (2005). Chemical characteristics of aerosols transported from Asia to the East China Sea: An evaluation of anthropogenic combined nitrogen deposition in autumn. *Atmospheric Environment*, *39*(9), 1749–1758. https://doi.org/10.1016/j.atmosenv.2004.11.037

O'Dowd, C. D., Maria Cristina, F., Fabrizia, C., Darius, C., Mihaela, M., Stefano, D., et al. (2004). Biogenically driven organic contribution to marine aerosol. *Nature*, *431*(7009), 676–680. https://doi.org/10.1038/nature02959

Palmer, P. I., & Shaw, S. L. (2005). Quantifying global marine isoprene fluxes using MODIS chlorophyll observations. *Geophysical Research Letters*, *32*(9), L09805. https://doi.org/10.1029/2005GL022592

Park, K.-T., Jang, S., Lee, K., Yoon, Y. J., Kim, M.-S., Park, K., et al. (2017). Observational evidence for the formation of DMS-derived aerosols during Arctic phytoplankton blooms. *Atmospheric Chemistry and Physics*, *17*(15), 9665–9675. https://doi.org/10.5194/acp-17-9665-2017

Park, K.-T., Lee, K., Kim, T.-W., Yoon, Y. J., Jang, E.-H., Jang, S., et al. (2018). Atmospheric DMS in the Arctic Ocean and its relation to phytoplankton biomass. *Global Biogeochemical Cycles*, *32*(3), 351–359. https://doi.org/10.1002/2017gb005805

Peng, X., Wang, W., Xia, M., Chen, H., Ravishankara, A. R., Li, Q., et al. (2021). An unexpected large continental source of reactive bromine and chlorine with significant impact on wintertime air quality. *National Science Review*, *8*(7), nwaa304. https://doi.org/10.1093/nsr/nwaa304

Quinn, P. K., Bates, T. S., Schulz, K. S., Coffman, D. J., Frossard, A. A., Russell, L. M., et al. (2014). Contribution of sea surface carbon pool to organic matter enrichment in sea spray aerosol. *Nature Geoscience*, *7*(3), 228–232. https://doi.org/10.1038/ngeo2092

Savoie, D. L., Arimoto, R., Keene, W. C., Prospero, J. M., Duce, R. A., & Galloway, J. N. (2002). Marine biogenic and anthropogenic contributions to non-sea-salt sulfate in the marine boundary layer over the North Atlantic Ocean. *Journal of Geophysical Research*, *107*(D18), 4356. https://doi.org/10.1029/2001jd000970

Savoie, D. L., & Prospero, J. M. (1989). Comparison of oceanic and continental sources of non-sea-salt sulfate over the Pacific-Ocean. *Nature*, *339*(6227), 685–687. https://doi.org/10.1038/339685a0

Simo, R., & Pedros-Alio, C. (1999). Role of vertical mixing in controlling the oceanic production of dimethyl sulphide. *Nature*, *402*(6760), 396–399. https://doi.org/10.1038/46516

Sorooshian, A., Crosbie, E., Maudlin, L. C., Youn, J. S., Wang, Z., Shingler, T., et al. (2015). Surface and airborne measurements of organosulfur and methanesulfonate over the western United States and coastal areas. *Journal of Geophysical Research - D: Atmospheres*, *120*(16), 8535–8548. https://doi.org/10.1002/2015JD023822

Spracklen, D. V., Arnold, S. R., Sciare, J., Carslaw, K. S., & Pio, C. (2008). Globally significant oceanic source of organic carbon aerosol. *Geophysical Research Letters*, *35*(12), L12811. https://doi.org/10.1029/2008gl033359

Stahl, C., Cruz, M. T., Bañaga, P. A., Betito, G., Braun, R. A., Aghdam, M. A., et al. (2020). Sources and characteristics of size-resolved particulate organic acids and methanesulfonate in a coastal megacity: Manila, Philippines. *Atmospheric Chemistry and Physics*, *20*(24), 15907–15935. https://doi.org/10.5194/acp-20-15907-2020

Stark, H., Brown, S. S., Goldan, P. D., Aldener, M., Kuster, W. C., Jakoubek, R., et al. (2007). Influence of nitrate radical on the oxidation of dimethyl sulfide in a polluted marine environment. *Journal of Geophysical Research*, *112*(D10), D10S10. https://doi.org/10.1029/2006jd007669

Stein, A. F., Draxler, R. R., Rolph, G. D., Stunder, B. J. B., Cohen, M. D., & Ngan, F. (2015). NOAA's HYSPLIT atmospheric transport and dispersion modeling system. *Bulletin of the American Meteorological Society*, *96*(12), 2059–2077. https://doi.org/10.1175/bams-d-14-00110.1

Sun, Y. L., Wang, Z. F., Du, W., Zhang, Q., Wang, Q. Q., Fu, P. Q., et al. (2015). Long-term real-time measurements of aerosol particle composition in Beijing, China: Seasonal variations, meteorological effects, and source analysis. *Atmospheric Chemistry and Physics*, *15*(17), 10149–10165. https://doi.org/10.5194/acp-15-10149-2015

Sunda, W., Kieber, D., Kiene, R., & Huntsman, S. (2002). An antioxidant function for DMSP and DMS in marine algae. *Nature*, *418*(6895), 317–320. https://doi.org/10.1038/nature00851

Tang, G., Zhang, J., Zhu, X., Song, T., Münkel, C., Hu, B., et al. (2016). Mixing layer height and its implications for air pollution over Beijing, China. *Atmospheric Chemistry and Physics*, *16*(4), 2459–2475. https://doi.org/10.5194/acp-16-2459-2016

van der A, R. J., Mijling, B., Ding, J., Koukouli, M. E., Liu, F., Li, Q., et al. (2017). Cleaning up the air: Effectiveness of air quality policy for SO_2 and NO_x emissions in China. *Atmospheric Chemistry and Physics*, *17*(3), 1775–1789. https://doi.org/10.5194/acp-17-1775-2017

Van Rooy, P., Drover, R., Cress, T., Michael, C., Purvis-Roberts, K. L., Silva, P. J., et al. (2021). Methanesulfonic acid and sulfuric acid Aerosol Formed through oxidation of reduced sulfur compounds in a humid environment. *Atmospheric Environment*, *261*, 118504. https://doi.org/10.1016/j.atmosenv.2021.118504

Vettikkat, L., Sinha, V., Datta, S., Kumar, A., Hakkim, H., Yadav, P., & Sinha, B. (2020). Significant emissions of dimethyl sulfide and monoterpenes by big-leaf mahogany trees: Discovery of a missing dimethyl sulfide source to the atmospheric environment. *Atmospheric Chemistry and Physics*, *20*(1), 375–389. https://doi.org/10.5194/acp-20-375-2020

Vrekoussis, M., Liakakou, E., Mihalopoulos, N., Kanakidou, M., Crutzen, P. J., & Lelieveld, J. (2006). Formation of HNO_3 and NO_3 in the anthropogenically-influenced eastern Mediterranean marine boundary layer. *Geophysical Research Letters*, *33*(5), L05811. https://doi.org/10.1029/2005gl025069

Wang, F., Chen, Y., Meng, X., Fu, J., & Wang, B. (2016). The contribution of anthropogenic sources to the aerosols over East China Sea. *Atmospheric Environment*, *127*, 22–33. https://doi.org/10.1016/j.atmosenv.2015.12.002

Wang, J., & Wang, J. (2017). Spartina alterniflora alters ecosystem DMS and CH_4 emissions and their relationship along interacting tidal and vegetation gradients within a coastal salt marsh in Eastern China. *Atmospheric Environment*, *167*, 346–359. https://doi.org/10.1016/j.atmosenv.2017.08.041

Wang, Q., Zhuang, G., Huang, K., Liu, T., Deng, C., Xu, J., et al. (2015). Probing the severe haze pollution in three typical regions of China: Characteristics, sources and regional impacts. *Atmospheric Environment*, *120*, 76–88. https://doi.org/10.1016/j.atmosenv.2015.08.076

Wang, X., Jacob, D. J., Fu, X., Wang, T., Breton, M. L., Hallquist, M., et al. (2020). Effects of anthropogenic chlorine on PM2.5 and ozone air quality in China. *Environmental Science & Technology*, *54*(16), 9908–9916. https://doi.org/10.1021/acs.est.0c02296

Wang, Y., Zhuang, G., Tang, A., Yuan, H., Sun, Y., Chen, S., & Zheng, A. (2005). The ion chemistry and the source of PM2.5 aerosol in Beijing. *Atmospheric Environment*, *39*(21), 3771–3784. https://doi.org/10.1016/j.atmosenv.2005.03.013

Wanninkhof, R. (1992). Relationship between wind speed and gas exchange over the ocean. *Journal of Geophysical Research*, *97*(C5), 7373–7382. https://doi.org/10.1029/92jc00188

Watts, S. F. (2000). The mass budgets of carbonyl sulfide, dimethyl sulfide, carbon disulfide and hydrogen sulfide. *Atmospheric Environment*, *34*(5), 761–779. https://doi.org/10.1016/S1352-2310(99)00342-8

Willis, M. D., Köllner, F., Burkart, J., Bozem, H., Thomas, J. L., Schneider, J., et al. (2017). Evidence for marine biogenic influence on summertime Arctic aerosol. *Geophysical Research Letters*, *44*(12), 6460–6470. https://doi.org/10.1002/2017gl073359

Yang, G.-P., Zhang, H.-H., Su, L.-P., & Zhou, L.-M. (2009). Biogenic emission of dimethylsulfide (DMS) from the North Yellow Sea, China and its contribution to sulfate in aerosol during summer. *Atmospheric Environment*, *43*(13), 2196–2203. https://doi.org/10.1016/j.atmosenv.2009.01.011

Yang, G.-P., Zhang, H.-H., Zhou, L.-M., & Yang, J. (2011). Temporal and spatial variations of dimethylsulfide (DMS) and dimethylsulfoniopropionate (DMSP) in the East China Sea and the Yellow Sea. *Continental Shelf Research*, *31*(13), 1325–1335. https://doi.org/10.1016/j.csr.2011.05.001

Yang, G.-P., Zhang, S.-H., Zhang, H.-H., Yang, J., & Liu, C.-Y. (2015). Distribution of biogenic sulfur in the Bohai Sea and northern Yellow Sea and its contribution to atmospheric sulfate aerosol in the late fall. *Marine Chemistry*, *169*, 23–32. https://doi.org/10.1016/j.marchem.2014.12.008

Yang, Z., Kanda, K., Tsuruta, H., and Minami, K. (1996). Measurement of biogenic sulfur gases emission from some Chinese and Japanese soils, *Atmospheric Environment*, *30*(13), 2399–2405. https://doi.org/10.1016/1352-2310(95)00247-2

Yuan, H., Wang, Y., & Zhuang, G. (2004). MSA in Beijing aerosol. *Chinese Science Bulletin*, *49*(10), 1020. https://doi.org/10.1360/03wb0186

Zang, B., Li, S., Michel, F. C., Li, G., Zhang, D., & Li, Y. (2017). Control of dimethyl sulfide and dimethyl disulfide odors during pig manure composting using nitrogen amendment. *Bioresource Technology*, *224*, 419–427. https://doi.org/10.1016/j.biortech.2016.11.023

Zhang, S. H., Yang, G. P., Zhang, H. H., & Yang, J. (2014). Spatial variation of biogenic sulfur in the south Yellow Sea and the East China Sea during summer and its contribution to atmospheric sulfate aerosol. *The Science of the Total Environment*, *488–489*, 157–167. https://doi.org/10.1016/j.scitotenv.2014.04.074

Zhao, H., Jiang, X., & Du, L. (2017). Contribution of methane sulfonic acid to new particle formation in the atmosphere. *Chemosphere*, *174*, 689–699. https://doi.org/10.1016/j.chemosphere.2017.02.040

Zheng, B., Tong, D., Li, M., Liu, F., Hong, C., Geng, G., et al. (2018). Trends in China's anthropogenic emissions since 2010 as the consequence of clean air actions. *Atmospheric Chemistry and Physics*, *18*(19), 14095–14111. https://doi.org/10.5194/acp-18-14095-2018

Zhou, S., Li, H., Yang, T., Chen, Y., Deng, C., Gao, Y., et al. (2019). Characteristics and sources of aerosol aminiums over the eastern coast of China: Insights from the integrated observations in a coastal city, adjacent island and surrounding marginal seas. *Atmospheric Chemistry and Physics*, *19*(16), 10447–10467. https://doi.org/10.5194/acp-19-10447-2019

Zhu, L., Nenes, A., Wine, P. H., & Nicovich, J. M. (2006). Effects of aqueous organosulfur chemistry on particulate methanesulfonate to non–sea salt sulfate ratios in the marine atmosphere. *Journal of Geophysical Research*, *111*(D5), D05316. https://doi.org/10.1029/2005jd006326

References From the Supporting Information

Ayers, G., Ivey, J., & Goodman, H. (1986). Sulfate and methanesulfonate in the maritime aerosol at Cape Grim, Tasmania. *Journal of Atmospheric Chemistry*, *4*(1), 173–185. https://doi.org/10.1007/BF00053777

Berresheim, H., Eisele, F. L., Tanner, D. J., Mcinnes, L. M., Ramseybell, D. C., & Covert, D. S. (1993). Atmospheric sulfur chemistry and cloud condensation nuclei (CCN) concentrations over the northeastern Pacific Coast. *Journal of Geophysical Research*, *98*(D7), 12701–12711. https://doi.org/10.1029/93jd00815

Jefferson, A., Tanner, D. J., Eisele, F. L., Davis, D. D., Chen, G., Crawford, J., et al. (1998). OH photochemistry and methane sulfonic acid formation in the coastal Antarctic boundary layer. *Journal of Geophysical*, *103*(D1), 1647–1656. https://doi.org/10.1029/97jd02376

Li, S. M., Barrie, L. A., Talbot, R. W., Harriss, R. C., Davidson, C. I., & Jaffrezo, J. L. (1993). Seasonal and geographic variations of methanesulfonic-acid in the Arctic troposphere. *Atmospheric Environment. Part A. General Topics*, *27*(17–18), 3011–3024. https://doi.org/10.1016/0960-1686(93)90333-T

Ryu, J.-H., Han, H.-J., Cho, S., Park, Y.-J., & Ahn, Y.-H. (2012). Overview of geostationary ocean color imager (GOCI) and GOCI data processing system (GDPS). *Ocean Science Journal*, *47*(3), 223–233. https://doi.org/10.1007/s12601-012-0024-4

Saltzman, E., Savoie, D., Prospero, J., & Zika, R. (1985). Atmospheric methanesulfonic acid and non-sea-salt sulfate at Fanning and American Samoa. *Geophysical Research Letters*, *12*(7), 437–440. https://doi.org/10.1029/GL012i007p00437

Saltzman, E. S., Savoie, D. L., Prospero, J. M., & Zika, R. G. (1986). Methanesulfonic acid and non-sea-salt sulfate in pacific air: Regional and seasonal variations. *Journal of Atmospheric Chemistry*, *4*(2), 227–240. https://doi.org/10.1007/bf00052002

Saltzman, E. S., Savoie, D. L., Zika, R. G., & Prospero, J. M. (1983). Methane sulfonic acid in the marine atmosphere. *Journal of Geophysical Research*, *88*(C15), 10897. https://doi.org/10.1029/JC088iC15p10897

Savoie, D., Prospero, J., Larsen, R., Huang, F., Izaguirre, M., Huang, T., et al. (1993). Nitrogen and sulfur species in Antarctic aerosols at Mawson, Palmer station, and Marsh (King George Island). *Journal of Atmospheric Chemistry*, *17*(2), 95–122. https://doi.org/10.1007/BF00702821

Sharma, S., Chan, E., Ishizawa, M., Toom-Sauntry, D., Gong, S. L., Li, S. M., et al. (2012). Influence of transport and ocean ice extent on biogenic aerosol sulfur in the Arctic atmosphere. *Journal of Geophysical Research*, *117*(D12), D12209. https://doi.org/10.1029/2011jd017074

Udisti, R., Bazzano, A., Becagli, S., Bolzacchini, E., Caiazzo, L., Cappelletti, D., et al. (2016). Sulfate source apportionment in the Ny-Ålesund (Svalbard Islands) Arctic aerosol. *Rendiconti Lincei. Scienze Fisiche e Naturali*, *27*(S1), 85–94. https://doi.org/10.1007/s12210-016-0517-7